



## Improving the technique of vitreous cryo-sectioning for cryo-electron tomography: Electrostatic charging for section attachment and implementation of an anti-contamination glove box

Jason Pierson<sup>a</sup>, José Jesús Fernández<sup>b,c</sup>, Erik Bos<sup>a,1</sup>, Shoaib Amini<sup>a</sup>, Helmut Gnaegi<sup>d</sup>, Matthijn Vos<sup>a,2</sup>, Bennie Bel<sup>e</sup>, Freek Adolfsen<sup>e</sup>, José L. Carrascosa<sup>b</sup>, Peter J. Peters<sup>a,f,\*</sup>

<sup>a</sup> Division of Cell Biology, The Netherlands Cancer Institute – Antoni van Leeuwenhoek Hospital, Plesmanlaan 121, 1066 CX Amsterdam, The Netherlands

<sup>b</sup> Centro Nacional de Biotecnología – CSIC, Campus Universidad Autónoma, Cantoblanco, 28049 Madrid, Spain

<sup>c</sup> Department of Computer Architecture, University of Almería, Almería 04120, Spain

<sup>d</sup> Diatome Ltd., PO Box 1164, CH-2501 Biel, Switzerland

<sup>e</sup> Simco (Nederland) B.V., P.O. Box 71, 7240 AB Lochem, The Netherlands

<sup>f</sup> Kavli Institute of Nanoscience, Delft University of Technology, Delft, The Netherlands

### ARTICLE INFO

#### Article history:

Received 22 July 2009

Received in revised form 2 October 2009

Accepted 5 October 2009

Available online 12 October 2009

#### Keywords:

Anti-contamination glove box

Electrostatic charging

Vitreous cryo-sections

Cryo-electron tomography

80S ribosome

### ABSTRACT

Cryo-electron tomography of vitreous cryo-sections is the most suitable method for exploring the 3D organization of biological samples that are too large to be imaged in an intact state. Producing good quality vitreous cryo-sections, however, is challenging. Here, we focused on the major obstacles to success: contamination in and around the microtome, and attachment of the ribbon of sections to an electron microscopic grid support film. The conventional method for attaching sections to the grid has involved mechanical force generated by a crude stamping or pressing device, but this disrupts the integrity of vitreous cryo-sections. Furthermore, attachment is poor, and parts of the ribbon of sections are often far from the support film. This results in specimen instability during image acquisition and subsequent difficulty with aligning projection images.

Here, we have implemented a protective glove box surrounding the cryo-ultramicrotome that reduces the humidity around and within the microtome during sectioning. We also introduce a novel way to attach vitreous cryo-sections to an EM grid support film using electrostatic charging. The ribbon of vitreous cryo-sections remains in place during transfer and storage and is devoid of stamping related artefacts. We illustrate these improvements by exploring the structure of putative cellular 80S ribosomes within 50 nm, vitreous cryo-sections of *Saccharomyces cerevisiae*.

© 2009 Elsevier Inc. All rights reserved.

### 1. Introduction

An important goal of structural biology is to visualize protein complexes within the cell using methods that involve a minimum of preparation-associated artifacts. In recent years, cryo electron tomography (cryo-ET) has taken the forefront for imaging large and stochastically variable structures with close-to-native preser-

vation; it is currently the best technique available for imaging cellular machinery *in situ* at molecular resolution (Lucic et al., 2005). The technique has been limited, however, to specimens that are less than ~500 nm thick. When cells of a greater thickness are imaged, the low contrast and signal-to-noise ratio (SNR) create problems with image interpretation and identification of macromolecules within the context of a cell. As a result, most of the literature on cryo-ET is related to isolated macromolecular complexes or organelles (Nicastro et al., 2006), relatively small cells (Henderson et al., 2007), or on the thin margins of extended cells (Medalia et al., 2002). If cryo-ET is to become the general tool of choice for biological imaging, then a suitable method to slice large cells and tissue must be established.

Vitreous cryo-sectioning with a diamond knife has shown considerable promise for slicing large cells and tissue (Dubochet et al., 1988). Its application to tomography, however, has been limited (Hsieh et al., 2002, 2006; Al-Amoudi et al., 2007; Millen et al.,

**Abbreviations:** Cryo-ET, cryo-electron tomography; EM, electron microscopy; RH, relative humidity.

\* Corresponding author. Address: Division of Cell Biology, The Netherlands Cancer Institute – Antoni van Leeuwenhoek Hospital, Plesmanlaan 121, 1066 CX Amsterdam, The Netherlands.

E-mail address: [p.peters@nki.nl](mailto:p.peters@nki.nl) (P.J. Peters).

<sup>1</sup> Present Address: Leiden University Medical Center, Department of Molecular Cell Biology, Section Electron Microscopy, P.O. Box 9600, 2300 RC Leiden, The Netherlands.

<sup>2</sup> Present Address: FEI Company, Achtseweg Noord 5, P.O. Box 80066, 5600 KA Eindhoven, The Netherlands.

2008; Salje et al., 2009) due to a number of technical obstacles (Hsieh et al., 2006; Marko et al., 2006). One such limitation is contamination, in the form of large crystals, which accumulate inside the microtome, on the support film of an electron microscopic (EM) grid, and the vitreous cryo-sections.

Attachment of the vitreous cryo-sections to an EM grid support film is another technical bottleneck that limits the areas of the section that are suitable for cryo-ET. Currently, the methods used for creating attachment involve mechanical forces, generated by either a stamping tool or a pressing device (Christensen, 1971; Frederik et al., 1982). Using these methods for attachment, damage in the form of large fissures or cracks can be observed (Hsieh et al., 2006), which alters the integrity of both the ribbon of vitreous cryo-sections and the individual sections.

In addition, mechanical pressing creates only a limited number of contacts between the support film and the vitreous cryo-sections, resulting in poor adhesion between the section and the support film. This hinders tomographic data collection, due to erratic movements of the sample during imaging (Sartori Blanc et al., 1998), especially at high tilt angles, which subsequently compromises the use of fiducials for tilt-series alignment. Finally, there is a high chance that the vitreous cryo-sections become completely detached from the grid during the transfer to the EM.

In the present study we have implemented an anti-contamination glove box to create a reduced humidity environment surrounding the cryo-ultramicrotome. We also introduce a novel attachment method using electrostatic charging in a dry cryo-ultramicrotomy chamber. Similar ideas have been introduced in the past (Tsuji et al., 1992; Koller, 1965) to circumvent section disruption, however, the application of such procedures has been minimal. Using our novel electrostatic charging technique we have: (1) increased the reliability and relative throughput of suitable vitreous sections for electron tomography and (2) retained proper cryo-section ribbon integrity. We illustrate our novel techniques by analysing putative cellular 80S ribosomes from *Saccharomyces cerevisiae*.

## 2. Materials and methods

### 2.1. Specimen preparation

*Saccharomyces cerevisiae* were harvested at mid to late log phase (OD<sub>600</sub> of ~1.5) in YEP medium (30 g/L Dextrose) and 5 g/L yeast extract supplemented with 20% Dextran (w/v) (from *Leuconostoc mesenteroides*, 35–45 kDa; Sigma Chemical, St. Louis), a medium in which we have established an unperturbed cellular growth rate. In addition, *S. cerevisiae* in its original culturing media as mentioned above (without the addition of Dextran prior to freezing) was taken as a control. Yeast suspensions were taken up into copper tubes (inner Ø 350 µm) as described (Studer et al., 2001), and vitrified using an EM-PACT2 high-pressure freezing machine (Leica Microsystems, Vienna). The pressure reached 2000 bar within 15 ms and had a nominal cooling rate of ~20,000 °C s<sup>-1</sup>. After freezing, the copper tubes were stored in liquid nitrogen.

### 2.2. Cryo-ultramicrotomy

A single copper tube was transferred to a pre-cooled (–150 °C) EM FC6 cryo-ultramicrotome (Leica Microsystems, Vienna) that was covered with an anti-contamination glove box or ‘Cryosphere’ (Leica Microsystems, Vienna) (Supplementary Fig. SF1). In addition, dry sodium hydroxide pellets and an influx of dry nitrogen gas were used to reduce the humidity further and create over-pressure within the chamber; the humidity within the chamber could be reduced to below 1% RH.

The copper tube containing the vitrified sample was trimmed to a square block-face with dimensions approximately 100 × 100 µm using a cryotrim-45 diamond blade (Diatome, Biel, Switzerland). Fiducial gold markers were attached to C-Flat™ EM grids CF-2/2–2C (Aurion, Wageningen, The Netherlands; Quispe et al., 2007) by successively floating them on 10 µL drops of 10 nm gold (diluted 1:60 in distilled water) (Aurion), PBS, and distilled water. The excess liquid was removed from the grid using filter paper and the grids were stored. We found that C-Flat support films were preferable as the support film remained flatter than the support film of carbon coated molybdenum or copper grids when submerged in liquid nitrogen (Supplementary Fig. SF2).

Ribbons of vitreous cryo-sections were produced at a nominal cutting feed of 30–50 nm at cutting speeds ranging from 1 to 100 mm/s; the first sections of the block-face were cut at a speed of 0.6–1 mm/s. If the surface-gliding properties were suitable (i.e. vitreous cryo-sections were not sticking to the knife, appeared ‘shiny’, and flat), then the speed was increased incrementally to 20, 50 mm/s and ultimately 100 mm/s, using a 35° cryo diamond knife (Diatome, Biel, Switzerland) with a clearance angle of 6°. The cutting speed was varied only to ease the collection of long vitreous section ribbons (~3 mm or longer). Ribbons of vitreous cryo-sections were attached to the pre-treated EM grids using two independent methods for comparison. In both methods the electrode was positioned ~10–20 mm from the knife.

### 2.3. Conventional attachment using stamping

A ribbon of vitreous cryo-sections (microtome feed setting 50 nm) was pulled from the knife-edge using an eyelash attached to a wooden dowel, placed on top of the EM grid, re-positioned on a smooth platform behind the knife and stamped using a polished metal stamping tool (Leica, Vienna, Austria) (Supplementary Movie SM1). The grid was transferred to a grid box (Gatan) and stored in liquid nitrogen.

#### 2.3.1. Electrostatic charging for attachment

A ribbon of vitreous cryo-sections was pulled from the knife-edge (as above) over the EM grid and attached using electrostatic charging (Supplementary Movie SM2). Charging was accomplished via a generator connected to an electrode positioned above the knife (approximately 10–20 mm from the diamond knife). During normal ionization the electrode emitted a high voltage negative direct current (DC), which created a strong negative field towards the ribbon of vitreous sections. Switching between ionization and electrostatic charging was controlled using foot pedals or a control box. During electrostatic charging, the electrical field (emitted from the electrode) was switched to a negative polarized, low voltage (kV range) field. The ribbons of vitreous cryo-sections acted as an isolator (non-conductive) and the negatively charged ions remained on the ribbon, therefore electrostatically attaching the ribbon to the support film of a grounded, conductive EM grid positioned beneath, and perpendicular, to the field of charging (Fig. 1). The entire electrostatic charging apparatus (CRION) has been incorporated into the Leica FC7 EM cryo-ultramicrotome (Leica Microsystems, Vienna), with equipment developed by Simco, Lochem, The Netherlands. After charging, the grid was transferred to a grid box (Gatan Inc., Pleasanton, CA) for storage in liquid nitrogen.

### 2.4. Cryo electron microscopy/tomography

#### 2.4.1. Single projection images

Vitreous cryo-sections were imaged using a Tecnai 12 TEM (FEI, Eindhoven, The Netherlands). Images were recorded at 120 kV at liquid nitrogen temperatures on a 4 × 4 kV FEI Eagle CCD camera (FEI, Eindhoven, The Netherlands).

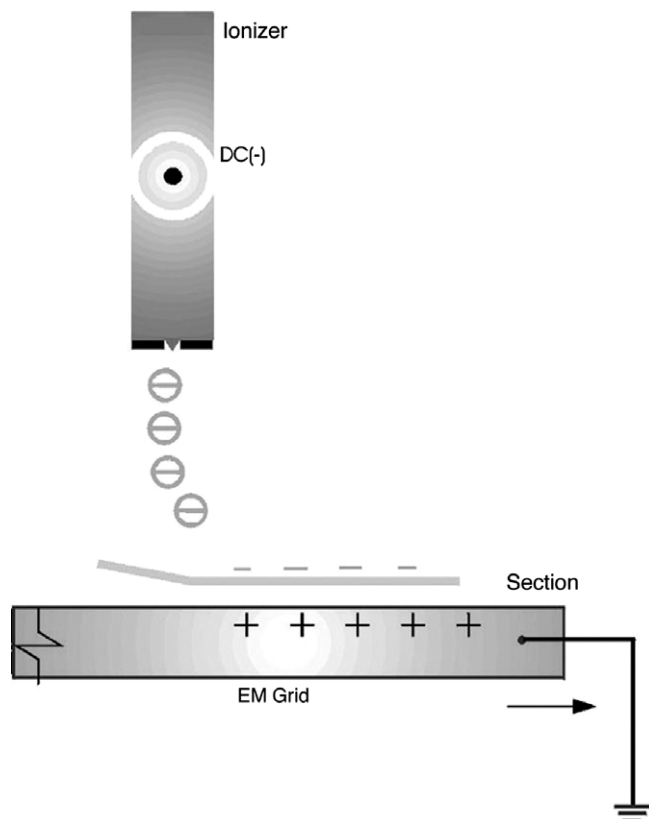


**Fig. 1.** A schematic drawing that shows the principle of electrostatic charging. At the top of the scheme is the electrode (ionizer). The electrode is connected to negative DC high voltage, which will create a strong negative ( $\ominus$ ) field. The rectangle at the bottom of the figure represents an EM grid, which is connected to ground through tweezers. Due to the fact that the ribbon, shown between the EM grid and the electrode, acts like an isolator (non-conductive) the negatively charged ions ( $\ominus$ ) remain on the ribbon of sections. The grounded EM grid is conductive and therefore an electrostatic force (attraction) between the negatively charged ribbon and the EM grid exists.

A nominal magnification of  $1900\times$ , with a 5.3 nm pixel size, was used for low magnification comparison between different attachment methods (electrostatic charging and stamping).

#### 2.4.2. High-resolution tomography

Ribbons of vitreous cryo-sections supported by EM grids were mounted in autoloader clips and inserted into the Titan autoloader

(FEI, Eindhoven, The Netherlands). Images were recorded at 300 kV, using a Titan cryo-TEM (Technical University of Eindhoven – TU/e, Eindhoven, The Netherlands) operated at liquid nitrogen temperatures equipped with a Gatan post column energy filter and a  $2 \times 2$  kV Gatan CCD camera (Gatan Inc., Pleasanton, CA.). Single axis tilt series were collected using FEI Xplore3D (FEI, Eindhoven, The Netherlands) acquisition program under low dose conditions. The angular tilt range was typically set from  $-65^\circ$  to  $+65^\circ$  with a  $1.5\text{--}2^\circ$  tilt increment, and an objective lens defocus of  $-4.5$  to  $-5.5$   $\mu\text{m}$ . Total dose was kept at or below  $\sim 100$   $e/\text{\AA}^2$  with a pixel size of 0.6 nm. Projection images were aligned using 10 nm gold fiducial markers on the EM support film and reconstructed (R-weighted back projection) using the IMOD package (Kremer et al., 1996). General visualization and surface rendering was performed using Amira (<http://amira.zib.de>).

#### 2.4.3. Subtomogram averaging

The structure of the 80S Ribosome from *S. cerevisiae* (Spahn et al., 2001) was taken from the EM Data Bank at the EBI (<http://www.ebi.ac.uk/pdbe/emdb/>) (entry emd-1076) and used as a template. A template-matching procedure was then applied to detect putative ribosomes within a binned version of the tomogram using Spider commands (Frank et al., 1996). False positives were discarded by visual inspection. Ribosome locations of 354 positive peaks were then extracted from the tomogram at full resolution. Angular determination and refinement were carried out as described (Ortiz et al., 2006; Brandt et al., 2009), using Bsoft tools (Heymann and Belnap, 2007). The resolution of the average ribosome was assessed based on the Fourier shell correlation (FSC) of two independent averages, each from half of the collected ribosomes (Ortiz et al., 2006).

## 3. Results

### 3.1. Reduced contamination vitreous cryo-sectioning

Contamination hampers all low temperature cryo-EM/ET techniques. In the case of low-temperature vitreous cryo-sectioning, the source is the air–nitrogen interface at the top of the microtome chamber (Supplementary Fig. SF3). In normal room humidity this interface can be compared to a ‘cloud’ that results in a blanket of contamination that covers the cryo-‘tools’ used inside the microtome, including the diamond knife (Fig. 2A).

To reduce contamination, a glove box was placed around the microtome (Supplementary Fig. SF1). In addition, we placed sodium hydroxide pellets inside the chamber and used a steady flow of dry nitrogen to further reduce the humidity. The dry nitrogen

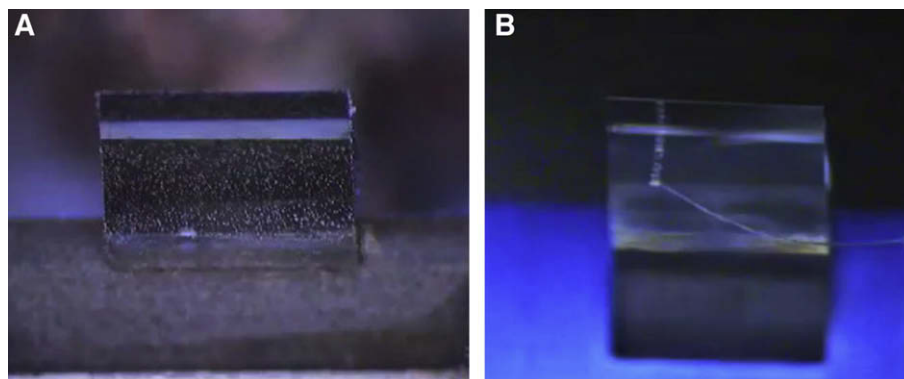


**Fig. 2.** Reducing contamination within the ultramicrotome at cryo-temperatures. (A) A diamond knife within an ultramicrotome at ambient humidity, which is heavily contaminated. (B) A diamond knife that is within an ultramicrotome that is surrounded by an anti-contamination glove box. The knife remains clean during vitreous cryo-sectioning.

flow creates an over-pressure within the chamber that maintains the low humidity when the glove box is opened to the outside environment. In this situation, the humidity can be reduced to below 1%. In this atmosphere, the air–nitrogen interface is not visible and the cryo-‘tools’, including the diamond knife, remain clean during vitreous cryo-sectioning (Fig. 2B).

### 3.2. Electrostatic charging

To facilitate cryo-ET of vitreous cryo-sections, the ribbon of sections must be well attached to the support film of an EM grid. Conventional stamping/pressing techniques compromise the integrity of the ribbon of vitreous cryo-sections. The force generated for attachment is not sufficient to retain the ribbon during storage in liquid nitrogen, and the vitreous cryo-sections are usually at a distance, from a few nanometers to micrometers, from the support film of the EM grid (Hsieh et al., 2006).

To circumvent these technical obstacles, a novel electrostatic charging procedure was developed to attach the sections to an EM grid support film. The complete apparatus consists of a generator, which applies a high voltage to an electrode, foot pedals to control the output of the generator, and a control box. The discharge mode produces an ionization current, which enhances the surface-gliding properties of the diamond knife during vitreous cryo-sectioning. The amplitude of ionization can be regulated either with a potentiometer or through external control. A charging mode is used for attaching the vitreous cryo-sections to an EM grid support film. When the generator is switched from discharge to charge, a burst of negative charge, approximately 1 s in duration, is produced in the vicinity of the electrode (Fig. 1), firmly attaching the sections to the support film. The detailed procedure is as follows: an EM grid is placed in the vicinity of the diamond knife (Fig. 3A). A relatively long ribbon of sections (denoted in Fig. 3B and C with white arrowheads) is pulled using an eyelash from the knife-edge over the EM grid (Fig. 3B). It is then attached using electrostatic charge (Fig. 3C) (also Supplementary Movie SM2). For proper attachment, the ribbon of sections must be above the EM grid, and the electrode tip must be normal to the plane of both

the ribbon of vitreous sections and the EM grid, and about 10–20 mm from the grid.

### 3.3. Attachment using electrostatic charging compared to conventional stamping

In our experience, stamping vitreous cryo-sections to an EM support film resulted in a number of mechanically induced artefacts in both the ribbon of sections and in the support film of the EM grid, reducing the number of suitable areas for tomography. The types of damage that were characteristically introduced by mechanical stamping/pressing-based attachment methods was prevented by using the electrostatic charging method (Fig. 3D and E). In addition, the charging procedure did not alter the vitreous state of the ice, as assessed by electron diffraction (Fig. 3F).

We have repeatedly seen that stamping was not sufficient to achieve good attachment of the ribbon of vitreous cryo-sections to the support film of an EM grid (Supplementary Movie SM1). After stamping, an eyelash was used to probe the interaction between the ribbon and the substrate. The ribbon was easily removed, suggesting that the method was not adequate for proper attachment. With electrostatic charging, the ribbon remained attached to the support film (Supplementary Movie SM2).

In order to quantify the success rate between the two attachment methods, comparison grids were produced under similar conditions (diamond knife, sample, ribbon length) using the stamping method and the electrostatic charging method. In every case where electrostatic charging was used for attachment, the ribbon was retained when observed in the EM. This was not the case, however, for the conventional stamping method. In a study of 5 grids that were prepared using the conventional stamping method, 2 out of the 5 were completely empty, even though the ribbon was observed in the microtome prior to transfer to the EM. This suggests that electrostatic charging increases the likelihood and reliability that a ribbon of vitreous cryo-sections will be present through transfer (in liquid nitrogen) and after insertion into the EM. ‘Coarse’ attachment and overall ribbon integrity was assessed

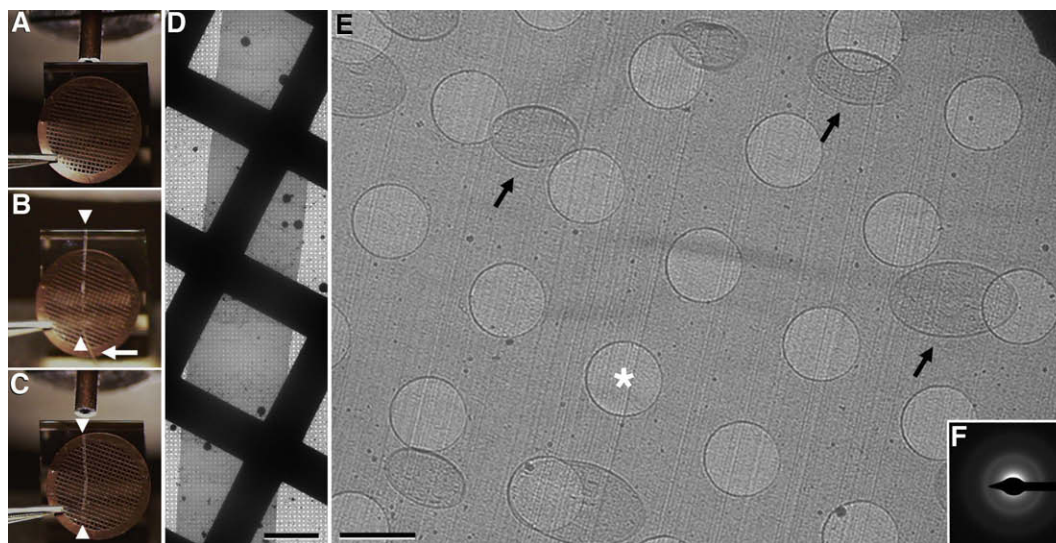


**Fig. 3.** Electrostatic charging technique for attaching a ribbon of vitreous sections to an EM support film. (A) An EM grid is placed at the diamond knife-edge using tweezers with a bent tip. (B) A ribbon of vitreous sections (white arrowheads) is guided over the EM grid using an eyelash (white arrow) attached to a wooden dowel. (C) Once the ribbon of vitreous sections is of suitable length (white arrowheads), approximately the diameter of the EM grid; the generator is switched from the discharge mode to the charge mode, causing the ribbon to attach to the EM grid. (D) A low magnification image showing the ribbon of vitreous sections after electrostatic charging. Scale bar = 50  $\mu\text{m}$ . (E) A medium magnification micrograph showing a vitreous section from within the ribbon. Note that the section is smooth and relatively flat with no apparent mechanically induced damage as is often seen with stamping/pressing techniques. *S. cerevisiae* cells can be seen scattered throughout the vitreous section (black arrows). Holes within the C-Flat EM grid can be seen and one such is denoted with a white asterisk. Scale bar = 2  $\mu\text{m}$ . (F) A selected area diffraction pattern confirming vitreous ice.

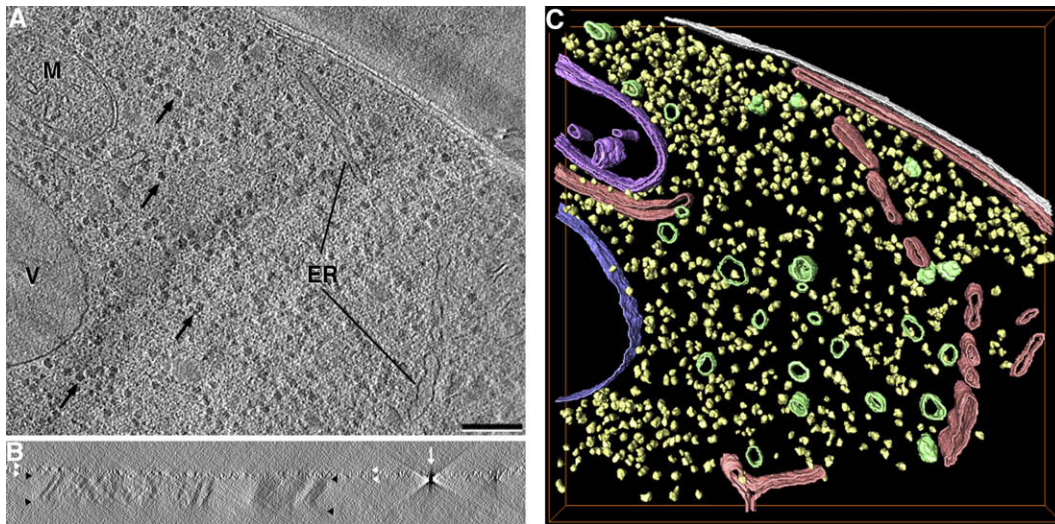


**Fig. 4.** Tomography of vitreous sections of *S. cerevisiae*. (A) 5-nm-thick tomographic slice from a vitreous section, (V) Vacuole, (M) Mitochondrion, (ER) Endoplasmic Reticulum, and black arrows indicate putative 80S ribosomes. Scale bar = 100 nm. (B) A flipped view (about the x-axis) from the tomographic reconstruction in (A). The vitreous section (black arrowheads) is well attached to the support film (white arrowheads). A fiducial gold marker is seen on the surface of the carbon support film (white arrow). Scale bar = 100 nm. (C) A surface rendered visualization of the tomographic volume in (A). Mitochondrion, purple; Vacuole, blue; Endoplasmic Reticulum, red; cell membrane, white; unidentified vesicle structures, green; unidentified macromolecular complexes including putative ribosomes, yellow.

using relatively low-magnification, tilted images, which can be seen in [Supplementary Fig. SF4](#).

#### 3.4. Tomography of *S. cerevisiae* vitreous sections

Tomography was performed on *S. cerevisiae* that were vitreous cryo-sectioned and collected using the novel electrostatic attachment method described above. Numerous tilt series were recorded and a representative tomogram can be seen in [Fig. 4](#). The ‘fine’ attachment was verified by flipping the volume around the x-axis ([Fig. 4B](#)), which directly shows that the vitreous section (black arrowheads) is well attached to the support film (white arrowheads). Alignment of individual projection images was accomplished using 10 nm gold fiducial markers applied to the surface of the carbon support film, our method of choice for tracking individual projection images within a tilt series for volumetric reconstruction. In the displayed tomogram, the residual mean error and standard deviation was below 1 pixel.

Specific cellular structures could be identified in a representative 5 nm slice from a tomographic reconstructed volume ([Fig. 4A](#)); a mitochondrion (M), profiles of the endoplasmic reticulum (ER), and a vacuole (V) are all evident. Large macromolecular complexes, such as putative 80S ribosomes, could also be recognized within the cell due to their inherent high contrast (black arrows).

We then focused on these *in situ* ribosome-like particles to illustrate the potential of the novel techniques proposed, deriving an average eukaryotic 80S ribosome map. The average ribosome map ([Fig. 5](#)) was computed by the standard combination of template matching and angular refinement ([Ortiz et al., 2006](#)), and had a resolution of 5.6 nm (FSC 0.5 criterion, see [Supplementary Fig. SF5](#)). The denoted ([Fig. 5A and B](#)) structural features that are recognizable from the 40S small subunit (40S) include the beak (bk) and the body (b). From the 60S large subunit (60S), the stalk base (SB) and the L1 protuberance (L1) are denoted ([Spahn et al., 2001](#)).

#### 4. Discussion

Cryo-ET of large cells and tissue can only be carried out after slicing these cells into thin sections. Tomography of vitreous sections, however, has been limited due to a number of technical bottlenecks ([Hsieh et al., 2006](#)). Here we have addressed the major difficulties; contamination in and around the microtome and attachment of the vitreous sections to an EM support film.

Frost contamination has been significantly reduced, by using a glove box surrounding the microtome to produce a controlled, low-humidity, environment. An unanticipated benefit of the environmental chamber was that ionizing properties of the electrode

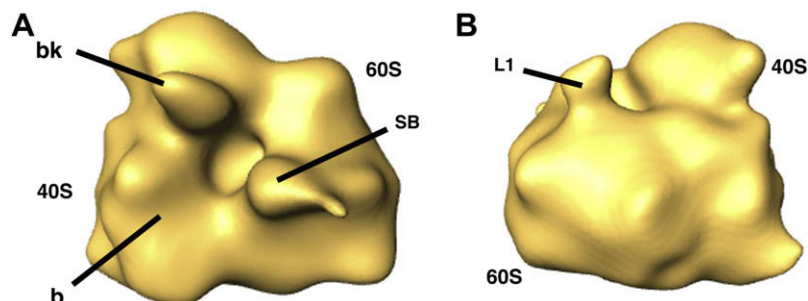


**Fig. 5.** 80S *S. cerevisiae* ribosome density map. (A) Specific 80S Ribosomal features can be recognized; the large 60S subunit (60S) and the associated stalk base complex L7/L12 region (SB), the small sub-unit (40S), beak region (bk) and base (b) region of the 40S. (B) A 90° rotated view from (A) that shows the L1 region of the 60S large sub-unit.

were observed to be more effective in a low humidity environment. In a normal room environment, the ionization electrode can become covered with ice contamination, which may reduce the electrical field strength from the electrode. When ionization is compromised, the surface-gliding properties of the diamond knife can be affected, making it difficult to produce high quality sections.

Attachment of vitreous cryo-sections to the support film of an EM grid has been problematic using conventional, force generating attachment methods, such as stamping or pressing. Although different techniques for mechanical attachment have been explored, none has yet been able to solve the attachment problem. Using electrostatic charging, the ribbon of vitreous sections is well attached to the EM grid support film, which increases the likelihood for successful tomography. Using conventional attachment methods, sections often moved or drifted during imaging due to the gap between the vitreous cryo-sections and the support film. With electrostatic charging, the sections are flush against the support film and therefore stable during imaging.

In addition, because the attachment has been improved using electrostatic charging, colloidal gold particles on the support film can be used as fiducial markers for tilt-series alignment. This is generally not the case with stamping. The poor attachment causes problems with aligning individual projection images from a tilt series to a common register because the section being imaged changes its position relative to the fiducial markers on the support film during tilting.

An alternative to using colloidal gold as fiducial markers is alignment through cross correlation-based algorithms (Castaño-Díez et al., 2007; Winkler and Taylor, 2006) that rely on tracking distinguishable features throughout the individual projection images. Cross correlation methods work relatively well when there is a high contrast and signal-to-noise within the images to facilitate feature tracking. Unfortunately, the inherent low contrast and signal-to-noise in cryo imaging techniques makes the tracking of distinguishable features rather difficult. In addition to cross correlation methods, there are procedures for applying fiducial markers directly onto the surface of the vitreous sections. Such methods include the use of Quatum Dots (Masich et al., 2006) and also colloidal gold particles as fiducial markers (Gruska et al., 2008). Unfortunately, vitreous sections are capricious during tilt series acquisition (Sartori Blanc et al., 1998), which can compromise the alignment as mentioned above. The most optimal situation may be to have tracking markers (quantum dots or colloidal gold) applied both to the surface of the vitreous sections, and to the support film.

In this study, the operator manually controlled the positioning of both the ribbon of vitreous cryo-sections and the EM grid prior to attachment. A more suitable method may employ a micromanipulator (Ladinsky et al., 2006), which would reduce the error of positioning. Using micromanipulation, a gentle tension can be maintained as the ribbon of vitreous cryo-sections is pulled from the knife-edge. Combining micromanipulation with electrostatic charging may be the most optimal technique.

Electron tomography already allows the identification of macromolecular complexes, together with analysis of their spatial distribution and their interactions in the native cellular context (Brandt et al., 2009). The electrostatic charging technique for attaching for vitreous sections to the EM grid for cryo-ET facilitates these studies on thin slices of biological specimens. As an illustrative example of the potential of this technique, the average eukaryotic ribosome *in situ* has been computed from a section of *S. cerevisiae*. This is the first step towards the construction of an 80S ribosomal map from a thin slice of a large eukaryotic cell, and towards identification of specific macromolecular spatial arrangements within the cellular context, as already revealed for

prokaryotic cells (Ortiz et al., 2006; Brandt et al., 2009). However, compression at the macromolecular level remains ambiguous and must be addressed in future studies. For future studies we must be fully confident that we only detect and select true cellular 80S ribosomes.

Although the resolution of the final ribosomal density map obtained here was sufficient to detect large structural landmarks on the 80S ribosome, increasing the particle pool may improve the resolution limits, as is commonly seen in single particle cryo-EM. We expect that these densities will be better defined in the near future, as the resolution within our density maps improve, and in combination with the rapidly expanding structural database for the 80S eukaryotic ribosome and its protein complexes.

## 5. Conclusions

The technique of vitreous cryo-sectioning still remains a challenge, however, the novel techniques presented here facilitate the procedure. We have shown that frost contamination is reduced inside the cryo ultramicrotome, when a protective anti-contamination glove box is used. We have also shown that electrostatic charging enhances attachment to an EM support film without compromising the integrity of ribbons of vitreous cryo-sections, so that the throughput of suitable areas for tomography can be increased compared to conventional methods. We obtained an initial glimpse of the putative 80S ribosomal cellular structure, within a thin vitreous cryo-section, when these novel improvements were applied to yeast cells.

## Acknowledgments

The authors thank Veronica M. Benito and the Fred van Leeuwen lab (NKI-AVL) for providing the yeast cells, the Bram Koster lab (LUMC, Leiden) for HPF, and Nico A.J.M. Sommerdijk and Gijsbertus de With (TU/e, Eindhoven) for use of the cryo-Titan. Special thanks to Peter Frederik (UM & TU/e), Jacques Neefjes (NKI-AVL), Sue Godsave (NKI-AVL), Reinhard Lihl (Leica-Microsystems, Vienna), and J. Richard McIntosh (University of Colorado, Boulder) for the ongoing discussions on the fundamentals of vitreous cryo-sectioning and cryo-EM and critical comments during the preparation of the manuscript. Computational resources were provided by the andalusian scientific computing center (CICA). We thank Alexander Griekspoor for assistance with the movies. Additional thanks to members of the NIMIC and NeCEN team. Work partially funded by grants: Food-CT-2006-023144 (P.P.), FP6-2006-Food-3B-023183 (P.P.), EU-LSHG-CT-2004-502828 (J.L.C.), MCI-BFU2008-02328 (J.L.C.), MCI-TIN2008-01117 (J.J.F.), JA-P06-TIC1426 (J.J.F.)

## Appendix A. Supplementary data

Supplementary data associated with this article can be found, in the online version, at doi:10.1016/j.jsb.2009.10.001.

## References

- Al-Amoudi, A., Díez, D.C., Betts, M.J., Frangakis, A.S., 2007. The molecular architecture of cadherins in native epidermal desmosomes. *Nature* 450, 832–837.
- Brandt, F., Etchells, S.A., Ortiz, J.O., Elcock, A.H., Hartl, F.U., Baumeister, W., 2009. The native 3D organization of bacterial polysomes. *Cell* 136, 261–271.
- Castaño-Díez, D., Al-Amoudi, A., Glynn, A.-M., Seybert, A., Frangakis, A.S., 2007. Fiducial-less alignment of cryo-sections. *J. Struct. Biol.* 159, 413–423.
- Christensen, A.K., 1971. Frozen thin sections of fresh tissue for electron microscopy with a description of pancreas and liver. *J. Cell Biol.* 51, 772–804.
- Dubochet, J., Adrian, M., Chang, J.-J., Homo, J.-C., Lepault, J., McDowell, A.W., Schultz, P., 1988. Cryo-electron microscopy of vitrified specimens. *Q. Rev. Biophys.* 21, 129–228.

- Frank, J., Radermacher, M., Penczek, P., Zhu, J., Li, Y., Ladjadj, M., Leith, A., 1996. SPIDER and WEB: processing and visualization of images in 3D electron microscopy and related fields. *J. Struct. Biol.* 116, 190–199.
- Frederik, P.M., Busing, W.M., Persson, A., 1982. Concerning the nature of the cryosectioning process. *J. Microsc.* 125, 167–175.
- Gruska, M., Medalia, O., Baumeister, W., Leis, A., 2008. Electron tomography of vitreous sections from cultured mammalian cells. *J. Struct. Biol.* 161, 384–392.
- Henderson, G.R., Gan, L., Jensen, G.J., 2007. 3-D ultrastructure of *O. Tauri*: electron cryotomography of an entire eukaryotic cell. *PLoS ONE* 8, e749. 13pp.
- Heymann, J.B., Belnap, D.M., 2007. Bsoft: image processing and molecular modeling for electron microscopy. *J. Struct. Biol.* 157, 3–18.
- Hsieh, C.-E., Marko, M., Frank, J., Mannella, C.A., 2002. Electron tomographic analysis of frozen-hydrated tissue sections. *J. Struct. Biol.* 138, 63–73.
- Hsieh, C.-E., Leith, A., Mannella, C.A., Frank, J., Marko, M., 2006. Towards high-resolution three-dimensional imaging of native mammalian tissue: electron tomography of frozen-hydrated rat liver sections. *J. Struct. Biol.* 153, 1–13.
- Koller, T., 1965. Mounting of ultrathin sections with the aid of an electrostatic field. *J. Cell Biol.* 27, 441–445.
- Kremer, J.R., Mastrorade, D.N., McIntosh, J.R., 1996. Computer visualization of three-dimensional image data using IMOD. *J. Struct. Biol.* 116, 71–76.
- Ladinsky, M.S., Pierson, J., McIntosh, J.R., 2006. Vitreous cryosectioning of cells, facilitated by a micromanipulator. *J. Microsc.* 224, 129–134.
- Lucic, V., Förster, F., Baumeister, W., 2005. Structural studies by electron tomography: from cells to molecules. *Annu. Rev. Biochem.* 74, 833–865.
- Marko, M., Hsieh, C.-H., Mannella, C.E., 2006. Electron tomography of frozen hydrated sections of cells and tissues. In: Frank, J. (Ed.), *Electron Tomography, Methods for Three-Dimensional Visualization of Structures in the Cell*, second ed. Springer, New York, pp. 49–81.
- Masich, S., Östberg, T., Norlén, L., Shupliakov, O., Daneholt, B., 2006. A procedure to deposit fiducial markers on vitreous cryo-sections for cellular tomography. *J. Struct. Biol.* 156, 461–468.
- Millen, J.I., Pierson, J., Kvam, E., Olsen, L.J., Goldfarb, D.S., 2008. The luminal N-terminus of yeast Nvj1 is an inner nuclear membrane anchor. *Traffic* 9, 1653–1664.
- Medalia, O., Weber, I., Frangakis, A.S., Nicastro, D., Gerisch, G., Baumeister, W., 2002. Macromolecular architecture in eukaryotic cells visualized by cryoelectron tomography. *Science* 289, 1209–1213.
- Nicastro, D., Schwartz, C., Pierson, J., Gaudette, R., Porter, M.E., McIntosh, J.R., 2006. The molecular architecture of axonemes revealed by cryoelectron tomography. *Science* 313, 944–948.
- Ortiz, J.O., Förster, F., Kürner, J., Linaroudis, A.A., Baumeister, W., 2006. Mapping 70S ribosomes in intact cells by cryoelectron tomography and pattern recognition. *J. Struct. Biol.* 156, 334–341.
- Quispe, J., Damiano, J., Mick, S.E., Nackashi, D.P., Fellmann, D., Ajero, T.G., Carragher, B., Potter, C.S., 2007. An improved Holey Carbon film for cryo-electron microscopy. *Microsc. Anal.* 13, 365–371.
- Salje, J., Zuber, B., Löwe, J., 2009. Electron cryomicroscopy of *E. coli* reveals filament bundles involved in plasmid DNA segregation. *Science* 323, 509–512.
- Sartori Blanc, N., Studer, D., Ruhl, K., Dubochet, J., 1998. Electron beam-induced changes in vitreous sections of biological samples. *J. Microsc.* 192, 194–201.
- Spahn, C.M., Beckmann, R., Eswar, N., Penczek, P.A., Sali, A., Blobel, G., Frank, J., 2001. Structure of the 80S ribosome from *Saccharomyces cerevisiae*-tRNA-ribosome and subunit-subunit interactions. *Cell* 107, 373–386.
- Studer, D., Graber, W., Al-Amoudi, A., Egli, P., 2001. A new approach for cryofixation by high-pressure freezing. *J. Microsc.* 203, 285–294.
- Tsuji, S., Anglade, P., Daudet-Monsac, M., Motelica-Heino, I., 1992. Cryoultramicrotomy: electrostatic transfer of dry ultrathin frozen sections on grids applied to the central nervous system. *Arch. Histol. Cytol.* 55, 423–428.
- Winkler, H., Taylor, K.A., 2006. Accurate marker-free alignment with simultaneous geometry determination and reconstruction of tilt series in electron tomography. *Ultramicroscopy* 106, 240–254.